Mineralogy and Petrology
https://doi.org/10.1007/s00710-022-00801-2

RESEARCH

Concerning the incorporation of potassium in the crystal structure of combeite ($Na_2Ca_2Si_3O_9$)

Volker Kahlenberg[1]

Received: 2 September 2022 / Accepted: 14 November 2022

Abstract

Potassium incorporation in the structure of combeite has been studied in detail. Since natural combeites are known to contain only small amounts of potassium focus was laid on the Na-rich part of a hypothetical solid-solution series with composition $Na_{2-x}K_xCa_2Si_3O_9$. Samples were prepared from mixtures of silica and the corresponding carbonates for nominal compositions with x = 0.2, 0.3 and 0.5, heated from ambient temperature to 1350 °C and slowly cooled to 1000 °C. After disintegration of the carbonates, the platinum capsules used as sample containers were welded shut in order to avoid losses of the volatile K_2O and Na_2O components. From all three batches potassium containing combeite crystals could be retrieved. Single-crystal diffraction experiments revealed the following compositions: $Na_{2.10(1)}K_{0.11(1)}Ca_{1.90(1)}Si_3O_9$, $Na_{2.09(1)}K_{0.18(1)}Ca_{1.91(1)}Si_3O_9$ and $Na_{2.13(1)}K_{0.18(1)}Ca_{1.87(1)}Si_3O_9$. Consistently, the trigonal crystals (space group $P\,3_1\,2\,1$) contained (i) (K + Na):Ca ratios larger than 1:1 and (ii) potassium concentrations lower than those in the starting mixtures. Since the K-contents of the samples obtained from the runs with x = 0.3 and 0.5 were almost identical, the solid-solution seems to be rather limited with an upper boundary of about one potassium atom per unit cell. The structure of the K-containing combeites is very close to the K-free structures reported in the literature. It can be described as a mixed tetrahedral-octahedral network in which additional K, Na and Ca cations are incorporated for charge compensation. A detailed analysis of the topological features of the net is presented. From the six observed extra-framework sites only the M22 position showing a coordination environment with ten next oxygen neighbours is involved in the K-substitution. Potassium uptake is also reflected in increasing values for the lattice parameters *a* and *c* as well as the unit-cell volumes. Actually, the *c*-axis is more affected from the incorporation of the comparatively large K^+-cations.

Keywords Combeite · Solid-solution · Potassium uptake · $Na_2Ca_2Si_3O_9$

Introduction

Combeite (idealized formula $Na_2Ca_2Si_3O_9$) is a rare highly-alkaline silicate mineral, whose formation requires very special petrological settings. It has been observed, for example, in lapilli and ashes of the only active carbonatite volcano on Earth, Ol Doinyo Lengai (Tanzania) (Dawson et al. 1989; Keller et al. 2010; Mitchell and Dawson 2012), in lavas and pyroclastic rocks from the Nyiragongo volcano range (Democratic Republic of the Congo) (Andersen et al. 2012), in the Ettringer Bellerberg volcano in the Eifel district (Germany) (Fischer and Tillmanns 1983) or in foidites occuring as porphyric dikes (Brava Island, Cape Verde) (Weidendorfer et al. 2016). According to the articles cited above, combeite is associated with minerals such as götzenite, wollastonite, clinopyroxene, nepheline, melilite, titanium-rich garnet, sodalite or aegirine.

The corresponding synthetic analogue with composition $Na_2O \times 2CaO \times 3SiO_2$ or NC_2S_3 (using the nomenclature of technical mineralogy) has been first mentioned by Morey and Bowen (1925). Köppen and Padurow (1958) suggested a rhombohedral unit cell, consistent with its optically uniaxial properties. About ten years later, indexed X-ray powder diffraction data of this phase have been published (Dent Glasser and Mileson 1968). At the same time there were also first indications that the chemical composition of the so-called "1:2:3-phase" is more complex involving a solid-solution

Editorial handling: M. Wildner

✉ Volker Kahlenberg
volker.kahlenberg@uibk.ac.at

[1] Institute of Mineralogy and Petrography, University of Innsbruck, Innrain 52, Innsbruck A-6020, Austria

series (Maki and Sugimura 1968). Furthermore, the same authors reported that $Na_2Ca_2Si_3O_9$ shows a reversible phase transition at about 485 °C. The existence of a continuous solid-solution series $Na_{3-x}Ca_{1.5+0.5x}Si_3O_9$ ($0 \le x \le 1$) was suggested by Moir and Glasser (1974). Finally, the crystal structures of both, the ambient and the high-temperature polymorph, have been studied using single-crystal diffraction (Ohsato and Takéuchi 1986; Ohsato et al. 1990; Fischer and Tillmanns 1987).

In the field of materials science, $Na_2Ca_2Si_3O_9$ has been intensively investigated as a crystalline phase in so-called 45S5 bioactive glass ceramics (Siqueira and Zanotto 2011; Xie et al. 2015; Blaeß et al. 2019; Karimi et al. 2018; Nawaz et al. 2020). Furthermore, the compound has been of interest as a potential host material for the preparation of red-emitting phosphors (Zhu et al. 2018), in the context of crystal nucleation and growth kinetics in soda-lime-glasses (Strnad and Douglas 1973; Macena et al. 2020) or as a phase occurring in steel slag glass–ceramics (Luo et al. 2020).

Data on the incorporation of alkali ions other than sodium into the crystal structure of combeite are rare. Natural samples from the Ol Doinyo Lengai locality, for example, contain only 0.13—0.50 wt.-% K_2O which is equivalent to 0.010 to 0.037 potassium atoms per formula unit. By contrast, whole rock analysis of the corresponding lavas resulted in K_2O-contents between 3.84 and 5.64 wt.-% (Klaudius and Keller 2006). Actually, mineral chemistry of the different species in the mineral assemblages indicates that nepheline is the primary potassium sink. A similar situation is observed when comparing combeites from the Nyiragongo area with the bulk chemistry of the nephelinite host rocks (Klaudius and Keller 2006). This leaves the question whether potassium cations can be incorporated into the combeite structure and, if so, to what extent. The aim of the present contribution was to bridge this gap in crystal-chemical knowledge. It is part of a wider ongoing research project on the phase relationships in the system Na_2O-K_2O-CaO-SiO_2.

Experimental details

In order to study the Na ↔ K substitution in the combeite structure, samples corresponding to a hypothetical solid-solution series $Na_{2-x}K_xCa_2Si_3O_9$ with $x = 0.2$, 0.3 and 0.5 have been prepared. For easy reference, these mixtures will be denoted K-Comb-n with $n = 2$, 3, 5, respectively. Starting materials were Na_2CO_3 (Merck, 99.9%), $CaCO_3$ (Merck, > 99.9%), K_2CO_3 (Alfa Aesar, 99.997%) and SiO_2 (AlfaAesar, 99.995%) which were dried for 24 h at 400 °C before weighing on an analytical balance. Subsequently, stoichiometric batches of 0.5 g each were thoroughly mixed in a planetary ball mill for 45 min at 600 rpm using ethanol as a milling fluid. After careful evaporation of the alcohol at 60 °C in a hot-air cabinet the educts were stored in a desiccator. Synthesis experiments were performed in small platinum capsules having an inner diameter of 5 mm and a length of approximately 35 mm. After closing the lower ends of each capsule using a welding apparatus, about 100 mg of the corresponding educts were charged into the Pt-tubes. The capsules were placed vertically in corundum combustion boats filled with alumina hollow spheres, transferred to a chamber furnace, heated slowly to 700 °C and annealed for 12 h for complete disintegration of the carbonates. After removing from the furnace, the solid material inside the tubes was carefully compacted with a fitting plastic bar. The upper open ends of the capsules were pinched and welded shut. Actually, sealing was performed in order to prevent K_2O and Na_2O losses which are likely to occur at elevated temperatures. Subsequently, the containers were placed back into the combustion boats and heated from 25 °C to 1350 °C with a ramp of 5 °C/min. After holding the target temperature for 1.5 h, the samples were cooled down to 1000 °C with a rate of 0.1 °C/min and, finally, quenched to ambient conditions by removing the alumina boats from the furnace. Weighing the closed capsules before and after the high-temperature treatment indicated that they had not leaked during the synthesis runs.

After opening the capsules, the solidified melt cakes were mechanically separated from the container, further crushed in an agate mortar and transferred to glass slides under a polarizing binocular. A first inspection revealed the presence of transparent, colorless-birefringent single crystals up to 250 µm in size embedded in a glassy matrix. The crystals showed sharp extinction between crossed polarizers. For each composition, between 5 and 8 crystals were fixed on glass fibers using nail hardener as glue. Preliminary X-ray diffraction data were collected on an Oxford Diffraction Gemini R Ultra single-crystal diffractometer equipped with a four-circle kappa-goniometer and a Ruby CCD detector. Measurements were conducted with Mo-K_α radiation. Initial diffraction experiments aiming on the determination of the unit-cell parameters proved the presence of combeite-related compounds. Within a single batch, only very minor variations concerning lattice parameters and cell volumes were observed pointing to a homogenous composition of the samples. Finally, the crystal with the best overall diffraction quality from each batch was selected for further structural investigations (see Table 1). The CrysAlisPRO software package (Rigaku Oxford Diffraction 2015) was employed to process the data. After indexing, the diffraction patterns were integrated. Further data reduction included Lorentz and polarization as well as an analytical numeric absorption correction using multifaceted crystal models.

Table 1 Crystal structure refinement details for the three crystals retrieved from the synthesis experiments K-Comb-2 to K-Comb-5

Crystal data			
Sample	K-Comb-2	K-Comb-3	K-Comb-5
Empirical formula	$Na_{2.10(1)}K_{0.11(1)}Ca_{1.90(1)}Si_3O_9$	$Na_{2.09(1)}K_{0.18(1)}Ca_{1.91(1)}Si_3O_9$	$Na_{2.13(1)}K_{0.18(1)}Ca_{1.87(1)}Si_3O_9$
Z	6	6	6
Formula weight (g/Mol)	2148.47	2160.48	2155.56
Space group	$P\,3_1\,2\,1$	$P\,3_1\,2\,1$	$P\,3_1\,2\,1$
Unit cell dimensions (Å)	$a = 10.4666(7)$	$a = 10.4972(6)$	$a = 10.4961(6)$
	$c = 13.1773(9)$	$c = 13.2333(8)$	$c = 13.2141(9)$
Volume (Å^3)	1250.17(15)	1262.83(13)	1260.74(13)
Density (calc., g/cm^3)	2.846	2.841	2.839
Absorption coefficient (mm^{-1})	1.938	1.960	1.939
F(000)	1063.6	1072.2	1069.6
Data collection			
Crystal size (mm^3)	0.098 × 0.149 × 0.171	0.089 × 0.110 × 0.163	0.160 × 0.213 × 0.238
θ-range for data collection	2.73 to 26.37°	3.81 to 26.36°	3.81 to 26.37°
Reflections collected	19848	20067	19891
Independent reflections	1698 [R(int) = 0.0457]	1725 [R(int) = 0.0494]	1721 [R(int) = 0.0467]
Refinement			
Refinement method	Full-matrix least-squares on F^2		
Data / restraints / parameters	1698 / 0 / 157	1725 / 0 / 157	1721 / 0 / 157
Goodness-of-fit on F^2	1.037	1.051	1.059
Final R indices [I > 2σ(I)]	R1 = 0.0306, wR2 = 0.0917	R1 = 0.0479, wR2 = 0.1311	R1 = 0.0479, wR2 = 0.1305
R indices (all data)	R1 = 0.0402, wR2 = 0.0954	R1 = 0.0520, wR2 = 0.1349	R1 = 0.0513, wR2 = 0.1341
Largest diff. peak and hole (e/Å^3)	1.506 and -1.133	1.463 and -0.891	1.473 and -0.947

All data collections were performed at 23(2) °C using Mo-K_α radiation

Diffraction symmetry of all crystals conformed to the trigonal Laue group $\bar{3}\,2/m$.

Initial coordinates for the structure refinements were taken from Fischer and Tillmanns (1987) using the same site nomenclature. Full-matrix least-squares refinements for all samples were performed with the program SHELXL (Sheldrick 2008) embedded in the software suite WinGX (Farrugia 1999). X-ray scattering factors were taken from the International Tables for Crystallography, Vol. C (Wilson 1995). The optimization calculations included fractional atomic coordinates and anisotropic displacement parameters. Allocation of the different cation species to the various non-tetrahedral cation sites was performed using a combination of site occupancy refinements and bond distance considerations. No constraints concerning the bulk chemistry of the crystals were applied. The refinements converged to residual values for R(|F|) between 3.10 and 4.80%. The largest shifts/esd in the final cycles were < 0.001. Notably, the resulting compositions were almost charge neutral. In comparison with the required six positive charges per formula unit that have to be contributed by the (Na + K + Ca)-cations the following values have been obtained: K-Comb-2: 6.01(2), K-Comb-3: 6.13(2) and K-Comb-5: 6.05(2). However, the formulas depart somewhat from ideal $Na_{2-x}K_xCa_2Si_3O_9$ and consistently exhibit less than two Ca- and more than two (Na + K)-atoms per formula unit (see Table 1). Due to the acentric character of the combeite structure, racemic twinning was taken into consideration. Actually, all samples represented inversion twins with volume ratios of the two individuals close to 1:1. Final coordinates, site occupancies as well as equivalent isotropic displacement parameters are given in Table 2. Anisotropic displacement parameters are listed in Table 3. Selected interatomic distances are summarized in Table 4. Figures showing structural features were prepared using the program VESTA3 (Momma and Izumi 2011). Bond valence sums (BVS) calculations have been performed with the program VaList (Wills 2010).

Results

The basic structural features of the three members of the solid-solution series are identical to those of pure K-free combeite (Ohsato and Takéuchi 1986; Fischer and Tillmanns 1987). According to the connectivity of the [SiO_4]-tetrahedra, the combeite-related compounds can be

Table 2 Atomic coordinates ($\times 10^4$), equivalent isotropic displacement parameters ($Å^2 \times 10^3$), site populations and bond valence sums (BVS) in valence units (v.u.)

	Wyckoff-position	x	y	z	U(eq)	Na, Ca and K-populations [%]	BVS [v.u.]
Si1	6*c*	1974(1)	1523(1)	7767(1)	9(1)		4.038
		1954(2)	1522(2)	7754(1)	9(1)		4.076
		1951(2)	1521(2)	7756(1)	11(1)		4.084
Si2	6*c*	4985(2)	3226(1)	8952(1)	9(1)		4.094
		4961(2)	3198(1)	8953(1)	9(1)		4.093
		4964(2)	3202(1)	8952(1)	11(1)		4.108
Si3	6*c*	6259(1)	1488(2)	7647(1)	9(1)		4.164
		6281(1)	1492(2)	7662(1)	9(1)		4.146
		6280(1)	1495(2)	7661(1)	10(1)		4.170
M1	6*c*	3095(2)	9834(1)	5928(1)	22(1)	61(1) Na / 39(1) Ca	1.302
		3146(2)	9870(2)	5918(1)	20(1)	67(1) Na / 33(1) Ca	1.248
		3141(2)	9868(2)	5922(1)	21(1)	66(1) Na / 34(1) Ca	1.250
M21	6*c*	5044(3)	3379(2)	6639(1)	26(1)	100 Na / 0 Ca	0.914
		5032(4)	3381(3)	6644(2)	24(1)	100 Na / 0 Ca	0.851
		5035(4)	3376(3)	6644(2)	26(1)	100 Na / 0 Ca	0.856
M22	3*a*	1647(10)	1647(10)	0	48(3)	22(1) K	1.418
		1677(8)	1677(8)	0	49(3)	36(1) K	1.458
		1656(8)	1656(8)	0	56(3)	36(1) K	1.446
M31	6*c*	5241(2)	3658(2)	1576(1)	23(1)	47(1) Na / 53(1) Ca	1.527
		5193(2)	3592(2)	1598(1)	31(1)	36(1) Na / 64(1) Ca	1.528
		5201(2)	3598(2)	1597(1)	31(1)	40(1) Na / 60(1) Ca	1.516
M32	3*b*	8211(1)	0	8333	11(1)	4(1) Na / 96(1) Ca	2.006
		8233(2)	0	8333	13(1)	12(1) Na / 88(1) Ca	1.848
		8235(2)	0	8333	13(1)	14(1) Na / 86(1) Ca	1.838
M4	3*a*	3059(1)	0	3333	9(1)	100 Ca	2.174
		3098(1)	0	3333	11(1)	100 Ca	2.138
		3096(1)	0	3333	13(1)	100 Ca	2.142
O1	3*b*	1640(5)	0	8333	21(1)		2.296
		1579(6)	0	8333	30(2)		2.288
		1587(6)	0	8333	31(2)		2.296
O2	3*b*	5586(5)	0	8333	25(1)		2.319
		5626(7)	0	8333	27(2)		2.320
		5628(7)	0	8333	28(2)		2.319
O3	6*c*	3446(3)	2823(4)	8357(2)	15(1)		2.240
		3437(4)	2776(5)	8343(2)	16(1)		2.295
		3439(4)	2785(5)	8345(2)	18(1)		2.240
O4	6*c*	5863(4)	2631(4)	8226(2)	17(1)		2.314
		5864(5)	2613(5)	8249(3)	22(1)		2.259
		5869(5)	2615(5)	8250(3)	23(1)		2.313
O5	6*c*	2421(4)	1484(4)	6614(2)	22(1)		2.034
		2367(5)	1428(5)	6608(3)	24(1)		1.935
		2373(5)	1439(5)	6612(3)	26(1)		1.954
O6	6*c*	4730(5)	2480(4)	30(2)	21(1)		2.046
		4683(6)	2467(4)	33(2)	23(1)		1.927
		4686(6)	2470(4)	33(2)	24(1)		1.946
O7	6*c*	5551(4)	1129(5)	6554(2)	23(1)		1.866
		5583(4)	1143(6)	6569(3)	26(1)		1.922
		5581(4)	1142(6)	6570(3)	26(1)		1.866
O8	6*c*	663(3)	1871(3)	7941(2)	15(1)		1.919
		690(4)	1924(4)	7928(3)	20(1)		1.922

Table 2 (continued)

	Wyckoff-position	x	y	z	U(eq)	Na, Ca and K-populations [%]	BVS [v.u.]
		687(4)	1919(4)	7926(3)	21(1)		1.919
O9	6*c*	5954(4)	4979(3)	8875(2)	22(1)		1.876
		5936(5)	4942(4)	8869(3)	24(1)		1.957
		5938(5)	4943(4)	8866(3)	26(1)		1.877
O10	6*c*	8006(3)	2202(4)	7772(2)	18(1)		1.913
		8026(4)	2248(6)	7785(3)	23(1)		1.865
		8023(4)	2247(6)	7783(3)	24(1)		1.889

U(eq) is defined as one third of the trace of the orthogonalized U_{ij} tensor. Lines one, two and three for each specific entry refer to the data of the samples K-Comb-2, K-Comb-3 and K-Comb-5, respectively

assigned to the group of cyclosilicates, consisting of elliptically distorted $[Si_6O_{18}]$-rings (see Fig. 1a). The relative orientation of up (U) and down (D) pointing apices of adjacent tetrahedra in the six-membered rings is UDUDUD. The site-symmetry of a single ring corresponds to the point group 2. The two-fold axis is running through the oxygen atoms O1 und O2. The rings are not planar but highly corrugated. In more detail, the Si atoms in the centers of the six tetrahedra are located close to the corners of a distorted cube with edge lengths ranging from 3.2 to 3.6 Å. Notably, the remaining two corners of the cube are occupied with Na/Ca-cations (see Fig. 1b).

Observed Si–O distances for the tetrahedra are in the normal range for oxidosilicates (Liebau 1985). As may be expected, the differences between the geometrical data of the tetrahedral units in the three samples are not pronounced. Consistently, bond lengths between Si and the bridging oxygen atoms (O1-O4) are considerably longer than the distances between Si and the corresponding non-bridging anions (O5-O10) (see Table 4). The tetrahedral O-Si–O angles show a significant scatter. For K-Comb-3, for example, the following values have been observed: 103.3–116.2° for Si1, 103.3–118.5° for Si2 and 104.2–119.5° for Si3, respectively. The polyhedral distortions can be quantified numerically with the quadratic elongation and the bond angle variance (Robinson et al. 1971). The relevant values have been included in Table 4.

Charge compensation within the structure is realized by the incorporation of Na-, K- and Ca-atoms which are distributed among a total of six different non-tetrahedral cation positions showing six (M1, M4), seven (M32, M31), eight (M21) and ten (M22) next oxygen neighbors.

Based on the previous investigation of Fischer and Tillmanns (1987), most of the M-sites were considered as mixed Na-Ca positions and the corresponding percentages were obtained from site population refinements. In summary, the M4-site is exclusively occupied with calcium, whereas M21 contains only sodium cations. M32 is Ca-dominated, while M1 and M31 show significant amounts of both sodium and calcium, respectively. Since the M22-O bond lengths (see Table 4) were considerably longer when compared with the other M–O distances, it was assumed that potassium is restricted to this position. A refinement of the corresponding site population, however, revealed that M22 is only partially occupied. Notably, our approach for allocating the different cation species to specific M-positions resulted in almost charge neutral chemical compositions without the need for the introduction of additional restraints in the refinements.

While the polyhedra around M1 and M4 can be described as distorted octahedra, the coordination environments of the remaining M-positions are more complex. For the present study, the M22-position is of special interest. Actually, it represents the barycenter of the largest void. The corresponding polyhedral volumes for the three samples vary between 47.4 and 47.9 $Å^3$. A projection of the whole structure parallel to [001] is given in Fig. 2.

Observed average M–O distances (see Table 2) compare well with literature values. Gagné and Hawthorne (2016) presented bond-lengths distributions and average bond distances of alkali and alkaline-earth cations bonded to oxygen as a function of the coordination number. Based on these data, the resulting "predicted" average bond distances using the refined values for the site populations for weighting were compared with the observed mean bond distances. For K-Comb-3, for example, the following values have been obtained (first entry: observed value / second entry: predicted value): M1: 2.468/2.418 Å; M21: 2.640/2.599 Å; M32: 2.473/2.459 Å; M4: 2.350/2.371 Å; M31: 2.516/2.481 Å; M22: 2.858/3.013 Å.

Bond valence sums for the cations and anions have been calculated using the parameter sets of Brown and Altermatt (1985) for Ca-O, Na–O and K–O as well as of Brese and O'Keeffe (1991) for Si–O interactions (see Table 2). Concerning the anions, it can be stated that the bridging oxygen atoms of the ring show a significant overbonding, whereas the non-bridging oxygens have bond valence sums which tend to be less but closer to the expected value of 2 valence units (v.u.). This feature is also observed for the

Table 3 Anisotropic displacement parameters ($Å^2 \times 10^3$)

	U_{11}	U_{22}	U_{33}	U_{23}	U_{13}	U_{12}
Si1	7(1)	6(1)	11(1)	0(1)	-2(1)	2(1)
	8(1)	6(1)	10(1)	-1(1)	-2(1)	1(1)
	10(1)	8(1)	12(1)	-1(1)	-2(1)	3(1)
Si2	9(1)	11(1)	9(1)	-2(1)	-2(1)	6(1)
	9(1)	13(1)	9(1)	-2(1)	-2(1)	8(1)
	10(1)	15(1)	10(1)	-2(1)	-2(1)	9(1)
Si3	11(1)	9(1)	8(1)	2(1)	3(1)	6(1)
	12(1)	7(1)	7(1)	2(1)	4(1)	6(1)
	13(1)	10(1)	9(1)	2(1)	4(1)	7(1)
M1	29(1)	16(1)	26(1)	-9(1)	-14(1)	16(1)
	27(1)	18(1)	19(1)	-9(1)	-11(1)	15(1)
	29(1)	19(1)	22(1)	-9(1)	-12(1)	16(1)
M21	21(1)	39(1)	20(1)	8(1)	1(1)	17(1)
	19(1)	43(1)	15(1)	10(1)	3(1)	20(1)
	19(1)	44(1)	19(1)	10(1)	3(1)	20(1)
M22	45(4)	45(4)	21(4)	-16(2)	16(2)	-3(4)
	43(3)	43(3)	21(3)	-16(2)	16(2)	-8(3)
	50(3)	50(3)	24(3)	-18(2)	18(2)	-7(3)
M31	19(1)	47(1)	13(1)	-11(1)	-5(1)	23(1)
	29(1)	68(1)	14(1)	-19(1)	-11(1)	38(1)
	28(1)	68(1)	15(1)	-19(1)	-11(1)	37(1)
M32	12(1)	15(1)	9(1)	-1(1)	-1(1)	7(1)
	13(1)	20(1)	7(1)	-3(1)	-1(1)	10(1)
	14(1)	21(1)	7(1)	-3(1)	-2(1)	10(1)
M4	12(1)	10(1)	6(1)	0(1)	0(1)	5(1)
	16(1)	11(1)	5(1)	-1(1)	-1(1)	6(1)
	17(1)	12(1)	7(1)	-1(1)	0(1)	6(1)
O1	14(2)	9(2)	39(3)	10(2)	5(1)	5(1)
	29(3)	16(3)	39(4)	12(3)	6(1)	8(2)
	27(3)	15(3)	46(4)	8(3)	4(1)	7(1)
O2	29(2)	16(3)	25(2)	13(2)	7(1)	8(1)
	39(3)	12(3)	20(3)	12(2)	6(1)	6(1)
	39(3)	15(3)	21(3)	14(2)	7(1)	8(1)
O3	12(2)	17(2)	16(2)	-2(1)	-6(1)	7(1)
	13(2)	21(2)	15(2)	-2(2)	-6(2)	9(2)
	13(2)	23(2)	18(2)	-3(2)	-7(2)	9(2)
O4	17(2)	15(2)	23(2)	-1(1)	5(1)	11(2)
	28(2)	23(2)	24(2)	-2(2)	7(2)	20(2)
	27(2)	22(2)	29(2)	-3(2)	6(2)	19(2)
O5	24(2)	31(2)	12(1)	-2(1)	-2(1)	15(2)
	30(3)	35(3)	10(2)	-6(2)	-6(2)	19(2)
	34(3)	38(3)	12(2)	-5(2)	-5(2)	22(2)
O6	28(2)	26(2)	11(1)	-2(1)	-4(1)	16(2)
	32(3)	30(2)	8(2)	1(1)	-6(2)	15(2)
	32(3)	32(2)	10(2)	-1(1)	-4(2)	18(2)
O7	27(2)	34(2)	14(1)	-3(2)	-4(1)	19(2)
	31(2)	36(3)	11(2)	2(2)	-5(2)	18(2)
	30(2)	37(3)	13(2)	-2(2)	-4(2)	19(2)
O8	12(2)	13(2)	21(2)	-1(1)	-2(1)	7(1)
	14(2)	23(2)	25(2)	-5(2)	-4(2)	12(2)
	14(2)	24(2)	26(2)	-6(2)	-4(2)	11(2)

Table 3 (continued)

	U_{11}	U_{22}	U_{33}	U_{23}	U_{13}	U_{12}
O9	26(2)	11(1)	25(2)	-5(1)	-8(2)	6(2)
	23(2)	14(2)	29(2)	-5(2)	-6(2)	4(2)
	26(2)	18(2)	28(2)	-4(2)	-5(2)	7(2)
O10	11(1)	20(2)	24(2)	1(2)	3(1)	7(1)
	10(2)	32(3)	24(2)	1(2)	5(1)	8(2)
	12(2)	32(2)	26(2)	-1(2)	3(1)	9(2)

The anisotropic displacement factor exponent takes the form: $-2\pi^2$ [$h^2a^{*2}U_{11}+\ldots+2$ h k a* b* U_{12}]. Lines one, two and three for each specific entry refer to the data of the samples K-Comb-2, K-Comb-3 and K-Comb-5, respectively

K-free combeite described by Fischer and Tillmanns (1987). The sums for the silicon cations compare well with the ideal value of 4 v.u. The mixed character of the sites M1 and M31 determined from the site occupancy refinements is also reflected in their bond valence sums. A strong positive deviation from the expected value of 1 v.u. is observed for the partially occupied M22-position. Even though the void around M22 is the largest available cavity, BVS-analysis shows that it is actually too small for hosting K^+. Notably, a calculation of the bond valences for M22 in the K-free combeite refined by Fischer and Tillmanns (1987) revealed, that the corresponding sodium cations on this position are subject to an extreme underbonding (0.534 v.u.), that is, in this case the cavity is too large.

Actually, the combeite structure type can be described as a mixed tetrahedral-octahedral framework built from the [SiO_4]- and [$M4O_6$]-units, that contains cavities of different sizes hosting the other cations. A detailed topological characterization of the mixed framework including coordination sequences and extended point symbols has been performed with the help of the program ToposPro (Blatov et al. 2014). Therefore, the framework is described by a graph composed of the vertices (T-sites containing Si1, Si2 and Si3, M4-site as well as O atoms) and edges(bonds) between them. The nodes of the graph can be classified according to their coordination sequences {N_k} (Blatov 2012). They represent a set of integers {N_k} ($k=1,..,n$), where N_k is the number of sites in the k-th coordination sphere of the T/M- or O- atom that has been selected to be the central one. The corresponding values for the symmetrically independent T-sites and the M4-position up to $n=12$ are summarized in Table 5. Furthermore, the extended point symbols (Blatov et al. 2010) listing all shortest circuits for each angle for any non-equivalent framework atom have been determined. These results are also given in Table 5.

Finally, the polyhedral microensembles or PME's have been constructed. On the lowest sublevel they are formed for each octahedron and tetrahedron in the asymmetric unit by considering all directly bonded [$M4O_6$]- and [SiO_4]-groups. They represent a geometrical interpretation of the coordination sequences up to the index $k=3$. The PME's of the first sublevel observed for the M4 nodes can be described as follows: each [$M4O_6$]-octahedron is immediately linked to six tetrahedra. Using the classification based on the calculation of the coordination sequences up to $k=3$ (Ilyushin and Blatov 2002) the PME's of M4 can be denoted as {6,6,18}. The PME's of all three crystallographically independent tetrahedral Si nodes conforms to {4,3,11} (see Fig. 3a and b).

Discussion

From a mineralogical point of view, combeite belongs to the so-called lovozerite-group of minerals (Pekov et al. 2009). The authors gave a comprehensive summary of the different members of the group including a detailed description of their structural characteristics. According to their analysis the lovozerite structure type is based on pseudo-cubic modules with edge lengths of about 7.5 Å. They distinguished non-tetrahedrally coordinated M, A and B cations which are located at the corners (M), the edge-centers (A) and the face-centers (B) of a single cube. Furthermore, so-called C-cations are mentioned which reside on one of the body-diagonals of a single cube. For the K-containing samples of this study the following allocations can be made: M = M4, A = M32/M31, B = M21/M22, C = M1 (see Fig. 4a). Notably, the barycenter of the smaller cube formed by the six Si-atoms of a single puckered ring and two additional M1-sites (see Fig. 1b) is located exactly in the center of the above-mentioned larger cube (see Fig. 4b).

So far, two other structure refinements of the ambient temperature polymorph of combeites have been published (Ohsato and Takéuchi 1986; Fischer and Tillmanns 1987). Though the samples employed in the previous investigations did not contain potassium, it is interesting to compare the results of the refinements in more detail. Ohsato and Takéuchi (1986) used a synthetic sample retrieved from a starting composition with a Na:Ca ratio of 1:1. Notably, for the refinement of the site-populations the bulk composition

Table 4 Selected bond lengths up to 3.0 [Å] and angles [°]

Bond distances			
Si1-O5	1.597(3)	Si1-O8	1.602(3)
	1.594(4)		1.597(4)
	1.589(4)		1.593(4)
Si1-O1	1.632(2)	Si1-O3	1.654(3)
	1.633(2)		1.647(4)
	1.633(2)		1.654(4)
Quadratic elongation	1.004	Bond angle variance	16.3
	1.004		18.4
	1.004		18.5
<Si1-O>	1.621		
	1.618		
	1.617		
Si2-O6	1.577(3)	Si2-O9	1.595(3)
	1.580(4)		1.593(4)
	1.579(4)		1.590(4)
Si2-O3	1.645(3)	Si2-O4	1.650(3)
	1.643(4)		1.651(4)
	1.642(4)		1.651(4)
Quadratic elongation	1.008	Bond angle variance	33.9
	1.008		32.8
	1.008		33.5
<Si2-O>	1.617		
	1.617		
	1.615		
Si3-O7	1.577(3)	Si3-O10	1.600(3)
	1.580(4)		1.600(4)
	1.576(4)		1.597(4)
Si3-O2	1.625(1)	Si3-O4	1.637(3)
	1.624(2)		1.642(4)
	1.626(2)		1.639(4)
Quadratic elongation	1.008	Bond angle variance	33.2
	1.007		31.7
	1.007		32.1
<Si3-O>	1.610		
	1.611		
	1.610		
M1-O6	2.319(3)	M1-O5	2.348(4)
	2.340(4)		2.348(4)
	2.337(4)		2.352(4)
M1-O7	2.375(3)	M1-O8	2.484(3)
	2.378(4)		2.502(4)
	2.378(4)		2.505(4)
M1-O9	2.511(3)	M1-O10	2.773(3)
	2.516(4)		2.725(4)
	2.515(4)		2.732(4)
<M1-O>	2.468		
	2.468		
	2.470		
M21-O5	2.455(5)	M21-O6	2.517(5)
	2.509(6)		2.572(7)
	2.502(6)		2.569(7)

Table 4 (continued)

M21-O4	2.529(4)	M21-O2	2.643(2)
	2.575(5)		2.649(2)
	2.571(5)		2.649(3)
M21-O7	2.674(5)	M21-O3	2.700(4)
	2.674(7)		2.683(4)
	2.680(7)		2.685(4)
M21-O7	2.663(5)	M21-O4	2.784(4)
	2.688(7)		2.771(5)
	2.680(7)		2.764(5)
<M21-O>	2.621		
	2.640		
	2.638		
M22-O3	2.726(7)	M22-O3	2.726(7)
	2.724(6)		2.724(6)
	2.733(6)		2.733(6)
M22-O1	2.790(4)	M22-O1	2.790(4)
	2.791(3)		2.792(3)
	2.784(3)		2.784(3)
M22-O6	2.892(9)	M22-O6	2.892(9)
	2.833(8)		2.833(8)
	2.851(9)		2.851(9)
M22-O5	2.977(2)	M22-O5	2.977(2)
	2.950(7)		2.950(7)
	2.945(8)		2.945(8)
M22-O8	2.952(3)	M22-O8	2.952(3)
	2.988(4)		2.988(4)
	2.984(4)		2.988(4)
<M22-O>	2.867		
	2.858		
	2.859		
M31-O7	2.284(3)	M31-O6	2.302(3)
	2.294(4)		2.310(4)
	2.292(4)		2.307(4)
M31-O3	2.428(4)	M31-O4	2.481(4)
	2.460(5)		2.502(6)
	2.458(5)		2.493(5)
M31-O10	2.565(4)	M31-O9	2.618(4)
	2.592(6)		2.674(5)
	2.584(6)		2.673(5)
M31-O9	2.827(4)		
	2.777(5)		
	2.776(5)		
<M31-O>	2.501		
	2.516		
	2.512		
M32-O5	2.296(3)	M32-O5	2.296(3)
	2.297(4)		2.297(4)
	2.297(4)		2.297(4)
M32-O8	2.380(3)	M32-O8	2.380(3)
	2.410(4)		2.410(4)
	2.406(4)		2.406(4)
M32-O10	2.530(4)	M32-O10	2.530(4)

Table 4 (continued)

	2.580(6)		2.580(6)
	2.582(6)		2.580(6)
M32-O2	2.747(6)		
	2.737(7)		
	2.736(7)		
<M32-O>	2.451		
	2.473		
	2.472		
M4-O9	2.315(3)	M4-O9	2.315(3)
	2.327(4)		2.327(4)
	2.329(4)		2.329(4)
M4-O10	2.326(3)	M4-O10	2.326(3)
	2.331(3)		2.331(3)
	2.330(3)		2.330(3)
M4-O8	2.391(3)	M4-O8	2.391(3)
	2.392(4)		2.392(4)
	2.389(4)		2.389(4)
<M4-O>	2.344		
	2.350		
	2.349		
O—Si—O angles			
O5-Si1-O8	115.94(17)	O5-Si1-O1	109.44(16)
	116.2(2)		109.0(2)
	116.0(2)		109.1(2)
O8-Si1-O1	111.5(2)	O5-Si1-O3	107.72(18)
	111.4(3)		108.8(2)
	111.8(3)		108.4(2)
O8-Si1-O3	107.28(17)	O1-Si1-O3	104.21(16)
	107.4(2)		103.3(2)
	107.4(2)		103.3(2)
O6-Si2-O9	118.68(18)	O6-Si2-O3	113.6(2)
	118.5(2)		113.3(3)
	118.7(2)		113.2(3)
O9-Si2-O3	104.00(19)	O6-Si2-O4	108.86(19)
	104.8(2)		109.3(2)
	104.6(2)		109.1(2)
O9-Si2-O4	104.1(2)	O3-Si2-O4	106.59(17)
	103.3(3)		106.6(2)
	103.2(3)		107.0(2)
O7-Si3-O10	119.72(17)	O7-Si3-O2	110.69(18)
	119.5(2)		110.7(2)
	119.5(2)		110.6(2)
O10-Si3-O2	103.7(2)	O7-Si3-O4	109.8(2)
	104.5(3)		109.9(3)
	104.4(3)		110.1(3)
O10-Si3-O4	104.94(19)	O2-Si3-O4	107.11(18)
	104.2(3)		107.2(2)
	104.2(3)		107.3(2)
Si—O—Si angles			
Si1-O1-Si1	148.2(3)	Si3-O2-Si3	174.7(4)
	151.3(5)		173.3(5)
	150.5(4)		173.0(5)

Table 4 (continued)

Si2-O3-Si1	145.6(2)	Si3-O4-Si2	159.8(2)
	148.4(3)		160.5(3)
	148.0(3)		160.4(3)

Distortion parameters for the tetrahedral units (quadratic elongation, bond angle variance) and average bond distances are also listed. Lines one, two and three for a specific entry refer to the data of the samples K-Comb-2, K-Comb-3 and K-Comb-5, respectively

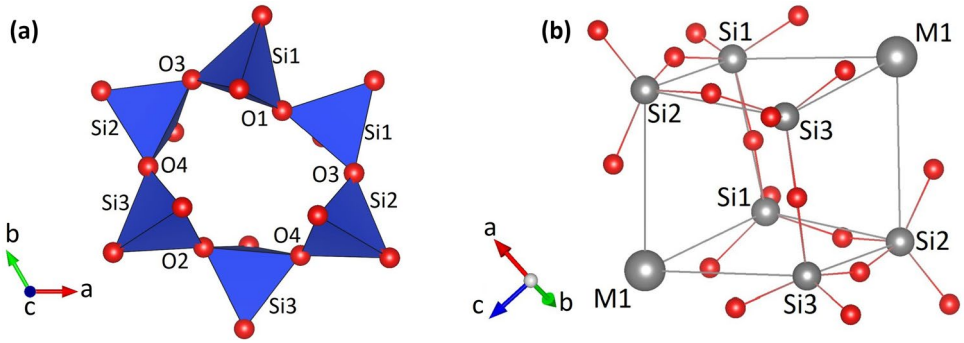

Fig. 1 A single six-membered $[Si_6O_{18}]$-ring in (**a**) a projection parallel [001] and (**b**) in a side view highlighting the pronounced corrugation. Oxygen atoms are given in red color. The six silicon atoms (small dark grey spheres) are located on the positions of a cube with edge-lengths of about 3.5 Å. The remaining two corners are occupied with atoms from the M1-site (large dark grey spheres). Edges of the distorted cube are indicated with grey lines

was constrained to be $Na_2Ca_2Si_3O_9$. Fischer and Tillmanns' study from 1987 was based on a natural crystal where microprobe analysis indicated a chemical composition of $Na_{2.2}Ca_{1.9}Si_3O_9$. With respect of the composition, the K-containing samples also show less than two Ca- and more than two (Na + K)-atoms per formula unit. Differences between the refinements can be also found concerning the sites into which the Na, Ca and K cations are incorporated. For example, Ohsato and Takéuchi (1986) did not observe any scattering density on the M22 site. For the samples studied in the present contribution as well as for the crystal characterized by Fischer and Tillmanns (1987), this position is partially occupied with K- or Na-ions, respectively. Consistently, all three investigations report the existence of more or less pronounced maxima in the difference Fourier maps close to some of the extra-framework M-sites. In the present study, the two highest peaks of residual scattering density for all three samples were observed about 0.8 Å away from the M1- and the M31-position, respectively. Due to their comparatively low absolute values of about 1.5 e/Å^3 it was decided not to include them into the refinements. Notably, Ohsato and Takéuchi (1986) preferred to split the M1 position, while Fischer and Tillmanns (1987) did not model any scattering density on their most significant maximum of 2.0 e/Å^3 in the vicinity the M1-position. In summary one can say, that the combeite structure type offers a quite large number of extra-framework positions which can be fully or partially occupied providing a large flexibility concerning the uptake of the sodium and calcium ions and, therefore, an appreciable range of stoichiometry.

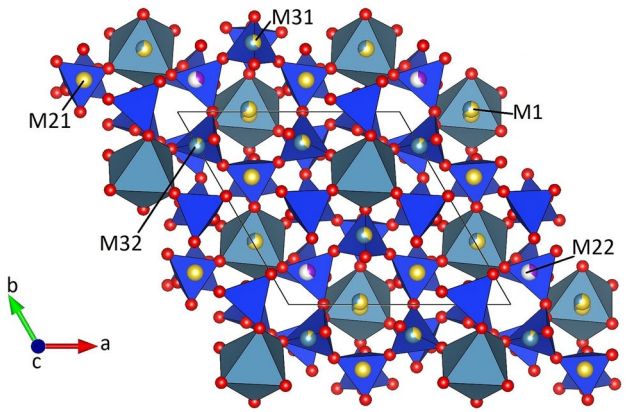

Fig. 2 Projection of the whole structure parallel to [001] for the sample K-Comb-3. $[SiO_4]$- and $[M4O_6]$-groups are indicated in dark and light blue. Smaller red spheres represent oxygen anions. Potassium (violet), sodium (yellow) and additional calcium (light blue) cations occupy voids between the tetrahedra and octahedra. Bi-colored spheres indicate mixed populations. The sizes of the bi-colored segments refer to the percentages determined from the site-occupancy refinements

The incorporation of potassium is also reflected in the unit-cell volumes. With respect to the lattice parameters given by Ohsato and Takéuchi (1986) the volume increases

Table 5 Coordination sequences $\{N_k\}$ of the tetrahedrally and octahedrally coordinated nodes as well as the extended point symbols for the combeite-type framework

T- or M-sites	Coordination sequences $\{N_k\}$ (k = 1,..,12)												Extended point symbol
	1	2	3	4	5	6	7	8	9	10	11	12	
T	4	3	11	9	31	21	64	36	109	53	152	78	12.12.12
M4	6	6	18	12	36	18	60	36	108	60	174	78	12.12.12.12.12.12.16.16.16 16.16.16.24_{16}.24_{16}.24_{16}

Notably, all symmetry independent T-sites (Si1, Si2, Si3) are topologically equivalent, that is, they have the same coordination sequences and extended point symbols

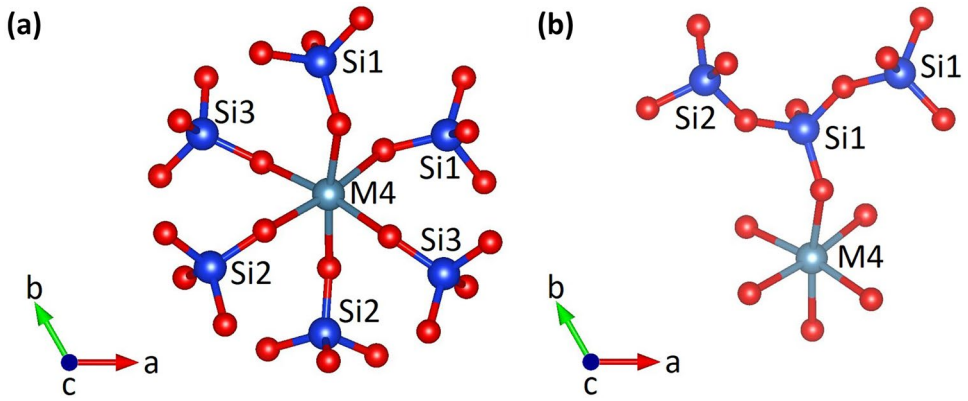

Fig. 3 Polyhedral microensembles of the crystallographically independent octahedral (M4) and one of the tetrahedral (Si) nodes: (**a**) {6,6,18} (for M4) and (**b**) {4,3,11} (identical for Si1, Si2 and Si3, respectively)

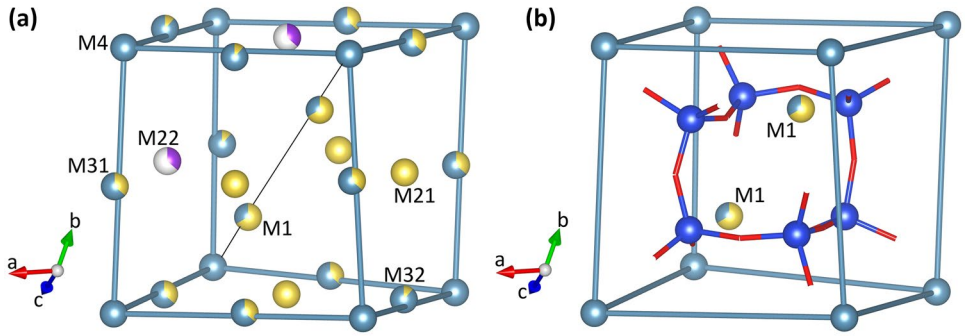

Fig. 4 (**a**) Fundamental cube of the cation arrangement in the combeite-type crystal structure of sample K-Comb-3. The edge-lengths of the cube are about 7.5 Å. (**b**) Location of a single puckered six-membered $[Si_6O_{18}]$-ring within the above-mentioned cube. For sake of clarity, cation sites residing on the edges and face centers have been removed

from 1248.7 Å^3 (K-free) to 1250.2 Å^3 (K-Comb-2) to 1262.8 Å^3 (K-Comb-3), that is—as might be expected—an increasing K-content leads to an increase in the unit-cell volumes. On the other hand, the two samples K-Comb-3 and K-Comb-5 having almost identical potassium contents exhibit a difference of about 2 Å^3 in the cell volumes (1262.8 as well as 1260.7 Å^3). By comparing the lattice parameters of a K-free combeite with one of the samples in this study, the so-called compositional strain (Ohasi and Burnham 1973) due to the potassium incorporation can be derived. Using the data sets of Ohsato and Takéuchi (1986) (a_0, c_0) as well as the sample K-Comb-3 (a_1, c_1) as reference points the following strain components can be derived:

$$\varepsilon_{11} = \varepsilon_{22} = \frac{a_1}{a_0} - 1 = 3.17 \cdot 10^{-3}$$

$$\varepsilon_{33} = \frac{c_1}{c_0} - 1 = 4.96 \cdot 10^{-3}$$

Actually, the potassium induced expansion of the combeite structure parallel to [001] is about 1.56 times larger than perpendicular to the c-axis.

Conclusions

With respect to the starting questions of this study one can say that the combeite structure can definitely host potassium cations. It is noteworthy, that in the three synthesis experiments of the hypothetical solid-solution $Na_{2-x}K_xCa_2Si_3O_9$ with starting compositions of x = 0.2, 0.3 and 0.5 the potassium concentrations of the resulting crystals were significantly less than the theoretical values from the educt mixtures (see Table 1). In addition, the crystals always contained more than two (K + Na)- and less than two Ca-cations. Even though the composition of the glassy matrix representing a former melt phase has not been analyzed it can be presumed that it must be enriched in potassium, because sealing of the capsules prevented any changes of the bulk composition which contained more K_2O-component than the resulting K-combeites.

The present structural study revealed that the potassium incorporation seems to be restricted to the partially occupied M22-site. If fully occupied, this would correspond to a total of 3 potassium ions per unit-cell. On the other hand, the two runs with initial compositions x = 0.3 and x = 0.5 resulted in almost identical potassium contents of x = 0.18 corresponding to about 1.1 potassium atoms per cell. This indicates, that—at least under the given synthesis conditions—this value corresponds to the upper potassium limit of the solid-solution series, i.e. there is no extensive Na ↔ K substitution. A possible explanation for the rather limited uptake of potassium in the combeite structure is related to the abovementioned strong overbonding of K^+ when incorporated on the M22-position, which is already the largest available cavity within the structure. At any rate, the K-concentrations of the combeite samples in this study are much higher than in those observed in natural samples (Klaudius and Keller 2006).

The limited Na–K-exchange may have also implications for thermodynamic modeling of the system K_2O-Na_2O-CaO-SiO_2. Actually, modeling calculations in this system are eagerly needed for a better understanding of the processes occurring in silicate-oxide slags and ashes forming during the combustion of biomass fuels. Up to now, the existence of only a handful of quaternary phases has been proven. $(K_{1.5}Na_{0.5})Ca_3Si_3O_{10}$ (Kahlenberg 2022), for example, seems to be isostructural with $K_2Ca_3Si_3O_{10}$ (Schmidmair et al. 2015). This implies the presence of a more extended solid-solution series $K_{2-x}Na_xCa_3Si_3O_{10}$ which adds additional complexity in thermodynamic calculations of the sub-solidus phase relationships and liquidus surfaces. For combeite, which shows a much more restricted solid-solution series, this problem is much less pronounced and the incorporation of potassium in modeling may be even neglected.

Acknowledgements The manuscript benefitted from the constructive reviews by Fernando Camara and Fabrizio Nestola as well as the helpful comments by editor Manfred Wildner.

Funding Open access funding provided by University of Innsbruck and Medical University of Innsbruck.

References

Andersen T, Elburg M, Erambert M (2012) Petrology of combeite- and götzenite-bearing nephelinite at Nyiragongo Virunga Volcanic Province in the East African Rift. Lithos 152:105–121

Blaeß C, Müller R, Poologasundarampillai G, Brauer DS (2019) Sintering and concomitant crystallization of bioactive glasses. Int J Appl Glass Sci 10:449–462

Blatov VA, O'Keeffe MO, Proserpio DM (2010) Vertex-, face-, point-, Schläfli-, and Delaney-symbols in nets, polyhedra and tilings: recommended terminology. CrystEngComm 12:44–48

Blatov VA (2012) Nanocluster analysis of intermetallic structures with the program package TOPOS. Struct Chem 23:955–963

Blatov VA, Shevchenko AP, Proserpio DM (2014) Applied topological analysis of crystal structures with the program package ToposPro. Cryst Growth Des. 14:3576–3586

Brese NE, O'Keeffe M (1991) Bond-valence parameters for solids. Acta Cryst B 47:192–197

Brown ID, Altermatt D (1985) Bond-valence parameters obtained from a systematic analysis of the Inorganic Crystal Structure Database. Acta Cryst B 41:244–247.

Dawson J, Smith JV, Steele IM (1989) Combeite ($Na_{2.33}Ca_{1.74}others_{0.12}$)$Si_3O_9$ from Oldoinyo Lengai, Tanzania. J Geol 97:365–372

Dent Glasser LS, Mileson JS (1968) Crystal data for $Na_2Ca_2Si_3O_9$. J Am Ceram Soc 51:55

Farrugia LJ (1999) WinGX suite for small-molecule single-crystal crystallography. J Appl Crystallogr 32:837–838

Fischer RX, Tillmanns E (1983) Die Kristallstrukturen von natürlichem $Na_2Ca_2Si_3O_9$ vom Mt. Shaheru (Zaire) und aus dem Mayener Feld (Eifel). N Jb Mineral Mh 49–59

Fischer RX, Tillmanns E (1987) Revised data for combeite, $Na_2Ca_2Si_3O_9$. Acta Cryst C 43:1852–1854

Gagné OV, Hawthorne FC (2016) Bond-length distributions for ions bonded to oxygen: alkali and alkaline-earth metals. Acta Crystallogr B 72:602–625

Ilyushin GD, Blatov VA (2002) Crystal chemistry of zirconosilicates and their analogs: topological classification of MT frameworks and suprapolyhedral invariants. Acta Crystallogr B 58:198–218

Kahlenberg V (2022) Crystal structure of $(K_{1.5}Na_{0.5})Ca_3Si_3O_{10}$. Acta Crystallogr E 78:727–731

Karimi AZ, Rezabeigi E, Drew RAL (2018) Crystallization behavior of combeite in 45S5 bioglass (R) via controlled heat treatment. J Non-Cryst Solids 502:176–183

Klaudius J, Keller J (2006) Peralkaline silicate lavas at Oldoinyo Lengai, Tanzania. Lithos 9:173–190

Keller J, Klaudius J, Kervyn M, Ernst GGJ, Mattson HB (2010) Fundamental changes in the activity of the natrocarbonatite volcano Oldoinyo Lengai, Tanzania. Bull Volcanol 72:893–912

Köppen N, Padurow NN (1958) Über die Kristallstruktur der Verbindung $Na_2O•2CaO•3SiO_2$. Naturwissenschaften 9:622

Liebau F (1985) Structural chemistry of silicates. Springer Verlag, Berlin, p 347

Luo ZH, He F, Zhang WT, Xiao YL, Xie JL, Sun RJ, Xie MQ (2020) Effects of fluoride content on structure and properties of steel slag glass-ceramics. Mater Chem Phys 242:122531

Macena GS, Abyzov AS, Fokin VM, Zanotto ED (2020) Off-stoichiometry effects on crystal nucleation and growth kinetics in soda-lime-silicate glasses. The combeite ($Na_2O.2CaO.3SiO_2$) – devitrite ($Na_2O.3CaO.6SiO_2$) joint. Acta Mater 196:191–199

Maki I, Sugimura T (1968) Metasilicates in the ternary system Na_2O-CaO-SiO_2. J Ceram Assoc Japan 76:144–148

Mitchell RH, Dawson JB (2012) Carbonate-silicate immiscibility and extremely peralkaline silicate glasses from the nasira cone and recent eruptions at Oldoinyo Lengai Volcano, Tanzania. Lithos 152:40–46

Moir GK, Glasser FP (1974) Phase equilibria in the system Na_2SiO_3-$CaSiO_3$. Phys Chem Glasses 15:6–11

Momma K, Izumi F (2011) VESTA 3 for three-dimensional visualization of crystal, volumetric and morphology data. J Appl Crystallogr 44:1272–1276

Morey GW, Bowen NL (1925) Ternary system sodium metasilicate – calcium metasilicate – silica. J Soc Glass Technol 9:226–264

Nawaz Q, de Pablos-Martin A, Silva JMDE, Hurle K, Jaimes ATC, Brauer DS, Boccaccini AR (2020) New insights into the crystallization process of sol-gel-derived 45S5 bioactive glass. J Am Ceram Soc 103:4234–4347

Ohasi Y, Burnham CW (1973) Clinopyroxene lattice deformations: the roles of chemical substitution and temperature. Am Mineral 58:843–849

Ohsato H, Takéuchi Y (1986) Structure of $Na_4Ca_4Si_6O_{18}$. Acta Cryst C 42:934–937

Ohsato H, Takéuchi Y, Maki I (1990) Structural study of the phase transition of $Na_4Ca_4Si_6O_{18}$. Acta Cryst B 46:125–131

Pekov IV, Krivovichev SV, Zolotarev AA, Yakovenchuk VN, Armbruster T, Pakhomovsky YA (2009) Crystal chemistry and nomenclature of the lovozerite group. Eur J Mineral 21:1061–1071

Rigaku Oxford Diffraction (2015) CrysAlisPRO, version 1.171.38.43. Oxford: Rigaku Oxford Diffraction

Robinson R, Gibbs GV, Ribbe PH (1971) Quadratic elongation: a quantitative measure of distortion in coordination polyhedra. Science 172:567–570

Schmidmair D, Kahlenberg V, Perfler L, Tribus M, Hildebrandt J, Többens DM (2015) On the ambient pressure polymorph of $K_2Ca_3Si_3O_{10}$ - an unusual mixed-anion silicate and its structural and spectroscopic characterization. J Solid State Chem 228:90–98

Sheldrick GM (2008) A short history of ShelX. Acta Cryst A 64:112–122

Siqueira RL, Zanotto ED (2011) Facile route to obtain a highly bioactive SiO_2–CaO–Na_2O–P_2O_5 crystalline powder. Mater Sci Eng C 31:1791–1799

Strnad Z, Douglas RW (1973) Nucleation and crystallization in the soda-lime-silica system. Phys Chem Glasses 14:33–36

Weidendorfer D, Schmidt MW, Mattson HB (2016) Fractional crystallization of Si-undersaturated alkaline magmas leading to unmixing of carbonatites on Brava Island (Cape Verde) and a general model of carbonatite genesis in alkaline magma suites. Contrib Mineral Petrol 171:43

Wills AS (2010) Program Valist. (http://fermat.chem.ucl.ac.uk/spaces/willsgroup/software/valist-bond-valence-calculations-listing/)

Wilson AJC (1995) International Tables for Crystallography, Volume C: Mathematical, Physical and Chemical Tables. 1st ed. Kluwer Academic Publishers, Dordrecht, Boston, London 883

Xie K, Zhang L, Yang X, Wang X, Yang G, Zhang L, Shao H, He Y, Fu J, Gou Z (2015) Preparation and characterization of low temperature heat-treated 45S5 bioactive glass-ceramic analogues. Biomed Glasses 1:80–92

Zhu Y, Tong C, Dai R, Xu C, Yang L, Li Y (2018) Luminescence properties of $Na_2Ca_2Si_3O_9$:Eu^{3+} phosphors via sol-gel method. Mater Lett 213:245–248